Photoluminescence and Raman Scattering from Catalytically Grown $Zn_xCd_{1-x}Se$ Alloy Nanowires

Rayapati Venugopal, Ping-I Lin, and Yit-Tsong Chen*

Department of Chemistry, National Taiwan University, Taipei 106, Taiwan, and Institute of Atomic and Molecular Sciences, Academia Sinica, P.O. Box 23-166, Taipei 106, Taiwan

Received: November 28, 2005; In Final Form: March 28, 2006

$Zn_xCd_{1-x}Se$ alloy nanowires, with composition $x = 0$, 0.2, 0.5, 0.7, and 1, have been successfully synthesized by a chemical vapor deposition (CVD) method assisted with laser ablation. The as-synthesized alloy nanowires, 60−150 nm in diameter and several tens of micrometers in length, complied with a typical vapor−liquid−solid (VLS) growth mechanism. The $Zn_xCd_{1-x}Se$ nanowires are single crystalline revealed from high-resolution transmission electron microscopic (HRTEM) images, selected area electron diffraction (SAED) patterns, and X-ray diffraction (XRD) measurement. Compositions of the alloy nanowires can be adjusted by varying the precursor ratios of the laser ablated target and the CVD deposition temperature. Crystalline structures of the $Zn_xCd_{1-x}Se$ nanowires are hexagonal wurtzite at $x = 0$, 0.2, and 0.5 with the [0 1 −1 0] growth direction and zinc blende at $x = 0.7$ and 1 with the [1 −1 1] growth direction. Energy gaps of the $Zn_xCd_{1-x}Se$ nanowires, determined from micro-photoluminescence (PL) measurements, change nonlinearly as a quadratic function of x with a bowing parameter of ∼0.45 eV. Strong PL from the $Zn_xCd_{1-x}Se$ nanowires can be tuned from red (712 nm) to blue (463 nm) with x varying from 0 to 1 and has demonstrated that the alloy nanowires have potential applications in optical and sensory nanotechnology. Micro-Raman shifts of the longitudinal optical (LO) phonon mode observed in the $Zn_xCd_{1-x}Se$ nanowires show a one-mode behavior pattern following the prediction of a modified random element isodisplacement (MREI) model.

1. Introduction

Band gap energy is one of the most important parameters that characterize a semiconductor and determines many gross electronic and optical properties. II−VI semiconductors with energy gaps covering the visible spectral range are compatible candidates for optoelectronic devices. In the past decade, considerable efforts were made to prepare nanoscaled II−VI semiconductors and to investigate their electronic and optical properties, because of their wide applications in photovoltaic,[1,2] electroluminescent,[3,4] and laser[5] devices. The promising advantages of II−VI materials, compared with other semiconductors, are their high photochemical stability and size-dependent optical properties due to quantum confinement effect.[6,7] Aside from choosing various semiconducting materials of different band gaps, it is now possible to control the band-gap energy of a given semiconductor from lowering its dimensionality and/or reducing its size to values comparable with or smaller than the corresponding excitonic Bohr diameter.[6]

Alloying of semiconductors is another means that can be applied to achieve semiconductor materials for various band-gap energies. Semiconducting alloys with high-emission quantum yields, low turn-on voltages, and high efficiency for energy conversion are of high applications in optoelectronic devices, such as semiconductor lasers and electromagnetic-radiation detectors. In particular, wide band-gap II−VI materials are a good representative example in laser photonics to generate coherent blue-green light. For example, the recently developed ZnSe-based laser diodes have a potential coverage of the whole green spectral region (490−590 nm).[7] The $Zn_xCd_{1-x}Se$ alloy is also commonly used as a quantum-well material in the ZnSe-based diodes grown on InP substrate which can effectively reduce the compressive strain. Due to the lattice matching of $Zn_xCd_{1-x}Se$ ($x \sim 0.5$) to the InP substrate, the $Zn_xCd_{1-x}Se$ quantum well can be applied as totally lattice-matched light emitters and is expected to be more reliable and resistant to strain-induced degradation. Different color emission can be achieved from almost identical structures where only the quantum-well thickness and/or composition are varied, which clearly shows the potential for these materials to fabricate integrated full-color display elements. ZnCdSe/BeZnTe alloy semiconducting multilayer structures have been applied to build laser diodes with a green-yellow emission range (550−600 nm).[8] Ternary/quaternary and quaternary/quaternary quantum layers of ZnCdSe/$Zn_xCd_yMg_{1-x}Se$ and ZnMgCdSe/ZnMgSeTe can also be integrated into light emitting diodes covering the visible spectral range.[9,10]

In addition to quantum wells, intense studies have been made toward one-dimensional II−VI semiconducting materials. For instance, binary nanowires of ZnSe[11−16] and CdSe[17−19] were synthesized with methods such as molecular-beam epitaxy (MBE),[12,16] metal organic chemical vapor deposition (MOCVD),[13,15] CVD assisted with laser ablation,[14,19] and wet chemistry[17,18] methods. Alloyed nanowires of ternary II−VI semiconductors with elementary compositions of ZnCdSe and ZnCdS,[20,21] successfully fabricated by MBE,[20] MOCVD,[21,22] and laser-assisted deposition,[23] are of high luminescence nature and well-crystalline structures and have been demonstrated to possess high lasing efficiency in a broad range of compositions.[23] In recent years, remarkable progress in the growth processes of nanocrystals has put alloy materials (III−V, II−VI, or IV) and their technology in a special category that

* To whom correspondence should be addressed. Tel: +886-2-2366-8238. Fax: +886-2-2362-0200. E-mail: ytchen@pub.iams.sinica.edu.tw.

10.1021/jp056892c CCC: $33.50
Published on Web 05/27/2006

promises versatile applications in photonic[24−26] and high-efficiency photovoltaic[27] devices.

In the $A_xB_{1-x}C$ mixed crystals of II−VI and III−V alloys, the nonlinear variation of energy gaps with composition (x) can generally be explained by the dielectric[28] and pseudopotential[29] models. While the dielectric model[28] considers the nonlinear variation of band gap with composition as due to fluctuations in the crystal field caused by the disorders in alloys, the pseudopotential model attributes the nonlinearity to nonlinear dependence of the crystal potential on the properties of component ions and neglects the disorder effect. For the phonons in a mixed crystal of an $A_xB_{1-x}C$ ternary alloy, there exist one-mode and two-mode behavior patterns.[30] In the one-mode type, phonon frequencies of single transverse optical (TO) and longitudinal optical (LO) modes in the $A_xB_{1-x}C$ mixed crystal vary continuously and approximately linearly with composition between the component frequencies of the end-member pure crystals (AC and BC). Furthermore, the strength of the mode remains approximately constant and the widths increase to a maximum at $x \approx 0.5$. In the two-mode type, on the other hand, two phonon frequencies for each of the allowed optic modes in the pure crystal are observed close to the frequencies of the end-members. In addition, the strength of each phonon mode of the mixed crystal is approximately proportional to the mole fraction of the component.

In view of the versatile optoelectronic properties of alloy semiconductors, $Zn_xCd_{1-x}Se$ ($0 < x < 1$) nanowires are good candidates to offer flexible physical parameters suitable for advanced nanotechnological applications. In this study, we have attempted to synthesize $Zn_xCd_{1-x}Se$ alloy nanowires, with the compositions of $x = 0$, 0.2, 0.5, 0.7, and 1, by a chemical vapor deposition (CVD) method assisted with laser ablation. Energy band gaps of the $Zn_xCd_{1-x}Se$ alloy nanowires, determined from micro-photoluminescence (PL) measurements, have shown a nearly linear dependence of composition (x) with a downward bowing. LO modes in the $Zn_xCd_{1-x}Se$ nanowires, observed in micro-Raman spectra, indicate that the LO phonon possesses a one-mode behavior pattern in the mixed crystal of $Zn_xCd_{1-x}Se$ nanowires.

2. Experimental Section

Catalytic Growth. Apparatus for the CVD experiment to synthesize $Zn_xCd_{1-x}Se$ nanowires is similar to that described in our earlier publications for the fabrications of Si nanowires[31] and CdSe nanobelts and nanosheets.[19] In the fabrications of CdSe and ZnSe nanowires, high-purity CdSe and ZnSe powders (Strem Chemicals, 99.999%) were used straightforwardly in the CVD experiments. For the syntheses of $Zn_xCd_{1-x}Se$ ($x = 0.2$, 0.5, and 0.7) alloy nanowires, the source materials were prepared first by physically mixing the desired quantities ($x = 0.2$, 0.5, and 0.7) of CdSe and ZnSe powders and then by sintering the mixture of CdSe and ZnSe powders at 1000 °C in a vacuum-sealed quartz tube for ~18 h. The sintered mixture was cooled slowly to room temperature in ~5 h and was then used as source material for the fabrication of $Zn_xCd_{1-x}Se$ alloy nanowires. The sintered mixture was pressed into a pellet and placed inside a quartz tube in the middle of an electric furnace. Prior to the synthetic reaction, the quartz tube was evacuated and heated to 825 °C. A gold (Au) film (20 nm thickness) coated on a Si wafer (~20 × 10 mm^2), used as a product collection substrate and located downstream to the carrier-gas flow at 550 °C, was vacuum annealed to recrystallize into Au nanoparticles. A carrier-gas mixture of Ar (90%) and H_2 (10%) with a flow rate of 200 sccm was subsequently introduced into the quartz tube until the pressure reached 250 Torr. When the gas flow became steady, a pulsed Nd:YAG laser (Spectra Physics, GCR-190) with 1064 nm wavelength, 7 ns pulse duration, 30 Hz repetition rate, and ~15 mJ/pulse was ignited to ablate the target of the sintered mixture. Furnace temperature was kept at 825 °C throughout the experiment. Colors for the as-synthesized products vary from dark brown (CdSe) to yellow (ZnSe) depending upon the composition (x) in the $Zn_xCd_{1-x}Se$ nanowires. It is found that the $Zn_xCd_{1-x}Se$ nanowires of various compositions were deposited at different collection positions, that is, at distinctive deposition temperature. Uniformity in the compositions of $Zn_xCd_{1-x}Se$ nanowires was sensitive to the growth temperature. By finely adjusting the growth temperature, the $Zn_xCd_{1-x}Se$ nanowires with a particular composition ($x = 0.2$, 0.5, or 0.7) could be found in a narrow area (~40 mm^2) on the substrate.

Electron Microscopic Characterizations. X-ray diffraction (XRD) spectra of the as-synthesized nanowires were recorded using Scintag × 1 diffractometer with Cu Kα ($\lambda = 1.5418$ Å) radiation at scanning speed of 2°/min in 2θ ranging from 20° to 60°. The fabricated nanostructures were also characterized by scanning electron microscopy (SEM) (LEO 1530, Filed Emission SEM), transmission electron microscopy (TEM), selected area electron diffraction (SAED), and high-resolution transmission electron microscopy (HRTEM) (JEOL JEM 2010 Analytical TEM at 200 kV and JEOL 4000 EX HRTEM at 400 kV). Compositions for the $Zn_xCd_{1-x}Se$ nanowires were measured by energy-dispersive X-ray spectroscopy (EDS) and energy-dispersive analysis of X-rays (EDAX) equipped in the TEM and SEM, respectively.

Confocal Spectroscopic Measurements. Experimental details for the PL and Raman spectroscopic measurements of nanoscaled materials studied in this laboratory can be found in some earlier publications.[19,32−34] In the present study, room-temperature PL from a single nanowire was measured in a confocal microscope (Jobin Yvon, MFO) using a 488-nm Ar−Kr ion laser (Coherent, Innova 70C) as an excitation source with laser intensity of ≤3.8 kW/cm^2. Laser light was introduced into a high objective lens (100×, NA = 0.9) to excite and collect the PL from a single nanowire. The PL signal was then sent into a monochromator (Jobin Yvon, Triax 550) via an optical fiber cable and was detected by a liquid-nitrogen cooled charge-coupled device (CCD) camera (Jobin Yvon, 1024 × 256 pixels). Room-temperature micro-Raman-scattering experiments were performed in a Nicolet Almega XR dispersive Raman spectrometer with a 180° backscattering geometry. The excitation light at 785 nm from a diode laser was focused to a spot of 4 μm in diameter by an optical microscope and was normal to a Si substrate on which the $Zn_xCd_{1-x}Se$ nanowires were freely dispersed. The backscattered Raman signal was then dispersed by a 1200 groove/mm grating and was finally collected by a thermoelectric-cooled Si CCD detector. In the micro-Raman measurements, laser intensity was kept ~9.3 kW/cm^2 to avoid any possible local heating effect. It is also noted that no significant band-shifts/broadenings were observed in the laser intensity of ≤50 kW/cm^2. This observation is consistent with our recent study of the Raman scattering from CdSe nanobelts and sheets,[19] where neither peak shift nor broadening effect was observed in the power-dependence measurements even with laser intensity up to 70 kW/cm^2.[35]

3. Results and Discussion

Structural Characterization. General SEM morphologies of the as-synthesized $Zn_xCd_{1-x}Se$ nanowires orienting randomly on the Si substrate are shown in parts a−e of Figure 1 with

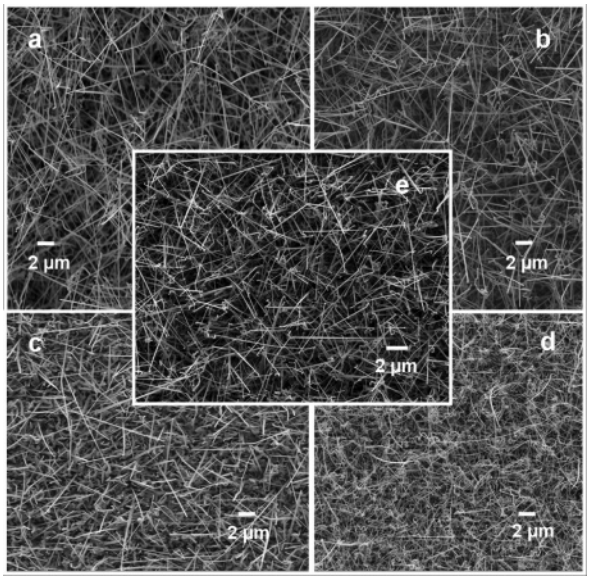

Figure 1. SEM images of the as-synthesized $Zn_xCd_{1-x}Se$ nanowires with (a) $x = 0$, (b) $x = 0.2$, (c) $x = 0.5$, (d) $x = 0.7$, and (e) $x = 1$.

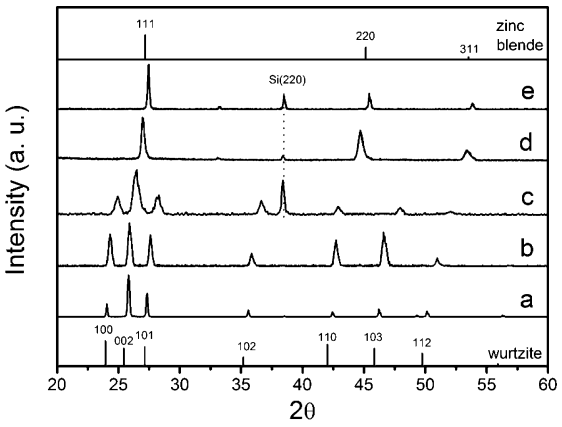

Figure 2. XRD spectra of (a) CdSe, (b) $Zn_{0.2}Cd_{0.8}Se$, (c) $Zn_{0.5}Cd_{0.5}Se$, (d) $Zn_{0.7}Cd_{0.3}Se$, and (e) ZnSe nanowires. Stick spectrum in the top (bottom) graph shows the XRD peaks for ZnSe (CdSe) powder, in which numbers indicate the Miller indices for the identified planes.

TABLE 1: Chemical Contents in the $Zn_xCd_{1-x}Se$ Nanowires with Various Compositions

	chemical contents from EDS		
composition (x)	Zn	Cd	Se
0	0	50.15	49.85
0.2	9.95	39.80	50.25
0.5	25.25	25.37	49.37
0.7	34.21	15.05	50.74
1	49.23	0	51.77

compositions $x = 0$, 0.2, 0.5, 0.7, and 1, respectively. While the diameters of the $Zn_xCd_{1-x}Se$ ($x = 0$, 0.2, 0.5, and 0.7) nanowires are distributed in the range of 70−150 nm, ZnSe nanowires in general have smaller diameters of 60−100 nm. Lengths for all of the $Zn_xCd_{1-x}Se$ ($0 \le x \le 1$) nanowires can be up to several tens of micrometers and respond sensitively to the synthetic reaction time. Chemical contents of the $Zn_xCd_{1-x}Se$ nanowires were analyzed from EDS data with their stoichiometric ratios being listed in Table 1.

Figure 2 displays typical XRD patterns for the $Zn_xCd_{1-x}Se$ nanowires with $x = 0$, 0.2, 0.5, 0.7, and 1, respectively. Stick spectra in the top and bottom graphs of Figure 2 are the XRD spectra of the ZnSe (zinc blende) and CdSe (wurtzite) source powders which have been assigned according to the standard PCDF WIN data. It is obvious that at $x = 0$, 0.2, and 0.5 (parts a−c in Figure 2), the $Zn_xCd_{1-x}Se$ nanowires are hexagonal wurtzite. In contrast, the structures can be identified zinc blende at $x = 0.7$ and 1 (parts d and e in Figure 2). The structural variation in the $Zn_xCd_{1-x}Se$ nanowires of this work is similar to the phase change in the bulky $Zn_xCd_{1-x}Se$ crystals at $0.6 < x < 0.8$ studied by Hotje et al.[36] The phase change in $Zn_xCd_{1-x}Se$ alloy nanowires was also reported recently by Shan et al.;[21] however, the change point is at $x < 0.13$, much lower than those in the bulky crystals[36] and of the present study, which could be attributed to the orientation effect of the GaAs (110) deposition substrate in the MBE growth process. It is noted that spectral widths in the XRD spectra of $Zn_xCd_{1-x}Se$ nanowires (Figure 2) are relatively sharp for the end-members ($x = 0$ and 1) and broader for those of $0 < x < 1$. This line width broadening might simply result from the contribution of a small range of compositions on the temperature-gradient CVD deposition substrate, when under the XRD measurement with a relatively large radiation-sampling area of ~1 cm^2. In contrast, the XRD spectra for the CdSe and ZnSe nanowires did not suffer from the uniform distribution of compositions, because both of these end-member nanowires were fabricated from their pure source powders in the CVD experiments.

Compared with the lattice constants of CdSe and ZnSe source powders, the interplanar distances analyzed from the XRD data (graphs a and e of Figure 2) reveal that there exist lattice contractions in both of the as-synthesized CdSe and ZnSe nanowires. We have measured $a/c = 4.271/6.898$ Å (CdSe nanowires) and 4.293/6.998 Å (CdSe powder) in the hexagonal wurtzite crystals and $a = 5.646$ Å (ZnSe nanowires) and 5.679 Å (ZnSe powder) for the zinc blendes. The observed lattice contractions could have been induced by a surface tension during surface reconstruction in the growth of nanocrystallites, which was also reported in the previous studies of CdSe nanocrystals[37] and CdSe nanobelts/nanosheets.[19] According to Vegard's law,[38,39] the lattice constants of $Zn_xCd_{1-x}Se$ nanowires with a hexagonal structure have to decrease as the Zn content increases due to the substitution of the Cd lattice by smaller Zn atoms. By the same token, the lattice constants of $Zn_xCd_{1-x}Se$ nanowires with a cubic structure have to increase with an increasing Cd content.

Typical TEM images of the $Zn_xCd_{1-x}Se$ ($x = 0$, 0.5, and 1) nanowires are shown in parts a, d, and g of Figure 3, respectively. In any as-synthesized $Zn_xCd_{1-x}Se$ nanowire, an Au-containing tip, composed of major Au and minor Zn, Cd, and Se, was always found at one end suggesting that the nanowires complied with a vapor−liquid−solid (VLS) growth mechanism and will be discussed later. Figure 3 also shows the SAED (parts b, e, and h) and HRTEM (parts c, f, and i) images of the $Zn_xCd_{1-x}Se$ ($x = 0$, 0.5, and 1) nanowires. The SAED patterns further reveal that single-crystalline $Zn_xCd_{1-x}Se$ nanowires have hexagonal wurtzite ($x = 0$, 0.2, and 0.5) and zinc blende ($x = 0.7$ and 1) structures. Lattice constants, growth directions, and lattice spacings calculated from the SAED and HRTEM data are listed in Table 2. Consistently, the lattice constants determined from the SAED data are in good agreement with the XRD results (Figure 2) discussed earlier.

Growth Mechanism. In this study, the formations of $Zn_xCd_{1-x}Se$ nanowires follow a vapor−liquid−solid (VLS) growth mechanism as evidenced by the eutectic tips containing Au, Zn, Cd, and Se. At an early reaction stage in the formation of $Zn_xCd_{1-x}Se$ nanowires, a vapor mixture of Zn, Cd, and Se was carried by the Ar and H_2 gases and deposited onto catalytic Au nanodroplets. When the dissolution of Zn, Cd, and Se in the Au nanodroplets became supersaturated, $Zn_xCd_{1-x}Se$ nano-

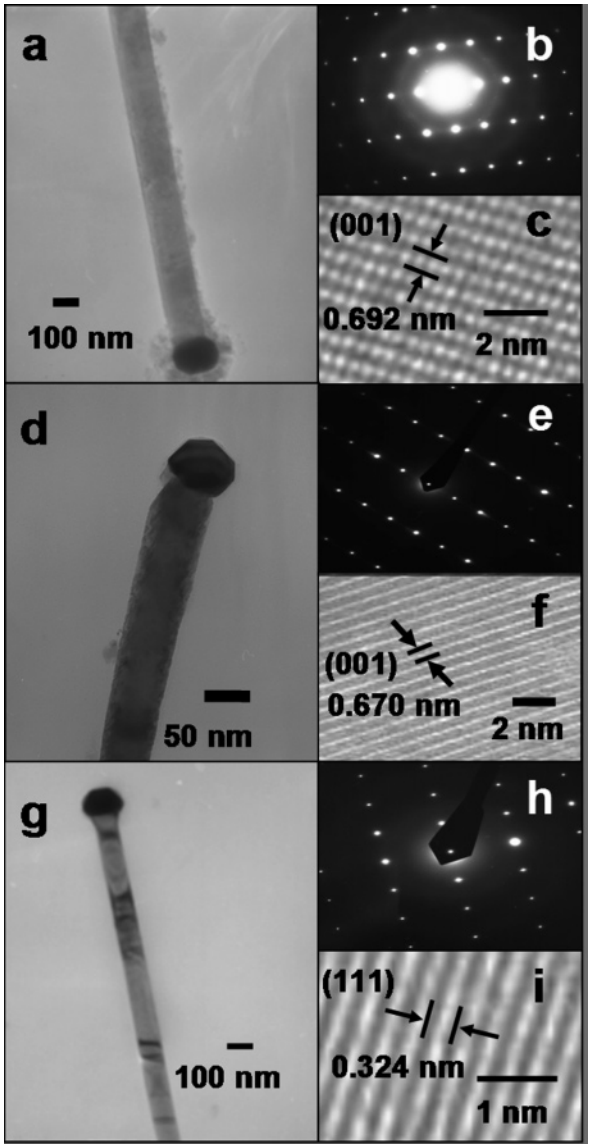

Figure 3. TEM, SAED, and HRTEM images of the as-synthesized CdSe (a, b, and c), $Zn_{0.5}Cd_{0.5}Se$ (d, e, and f), and ZnSe (g, h, and i) nanowires.

wires extruded from the liquid eutectic Au nanodroplets and precipitated at the liquid−solid interface. This process complies basically with an ordinary VLS growth model proposed originally by Wagner et al.,[40] in which a liquid cluster of metal catalyst provides energetically favored sites for the absorption/adsorption of gas-phase reactants.[31] The sizes of the catalysts are considered to be responsible for the diameters of resultant nanowires. Growth directions of the $Zn_xCd_{1-x}Se$ nanowires are listed in Table 2 which can be categorized into two groups. While one follows the [0 1 −1 0] direction of hexagonal wurtzite crystal at the compositions of $x = 0$, 0.2, and 0.5, the other is along the [1 −1 1] direction of the zinc blende structure at $x = 0.7$ and 1. These results suggest that the $Zn_xCd_{1-x}Se$ alloy nanowires prefer a specific crystalline structure with a particular growth direction at certain composition ratios and growth temperature. The growth directions for the end-members, that is, CdSe and ZnSe nanowires, are the same as those of CdSe nanobelts[19] and ZnSe nanowires prepared previously by the vapor phase reaction[11] and MBE[16] techniques.

Photoluminescence and Energy Gap. While both CdSe ($E_g = 1.74$ eV) and ZnSe ($E_g = 2.68$ eV) are direct band-gap materials, CdSe has high PL yield upon photoexcitation. In this study, the as-synthesized $Zn_xCd_{1-x}Se$ alloy nanowires exhibit strong PL at room temperature. Figure 4a shows the micro-PL spectra of $Zn_xCd_{1-x}Se$ nanowires, demonstrating clearly that the energy gaps of $Zn_xCd_{1-x}Se$ nanowires become wider as the Zn composition increases. On the basis of the strong PL yield of CdSe, micro-PL from single nanowires has been made possible for the $Zn_xCd_{1-x}Se$ nanowires of $x = 0$, 0.2, and 0.5, respectively, at 712, 667, and 591 nm (Figure 4a). In contrast, micro-PL from $Zn_xCd_{1-x}Se$ nanowires of $x = 0.7$ and 1 has relatively lower PL yields at 539 and 463 nm, respectively, for which the PL spectra could only be obtained by measuring a pile of nanowires.

Energy gaps for the $Zn_xCd_{1-x}Se$ nanowires of 1.74 ($x = 0$), 1.86 ($x = 0.2$), 2.10 ($x = 0.5$), 2.30 ($x = 0.7$), and 2.68 eV ($x = 1$), calculated from the observed PL peaks, are shown in Figure 4b as a function of composition (x). Variation of the energy gaps deviates slightly from linear dependence, displaying a downward bowing, which has also been reported as a general character for many thin films of II−VI alloy semiconductors.[41,42] The nonlinear variation of the energy gaps can be represented as a function of composition

$$E_g(x) = E_{BC} + (E_{AC} - E_{BC} - b)x + bx^2 \qquad (1)$$

where $E_g(x)$ is the energy gap of the $A_xB_{1-x}C$ mixed crystal, E_{AC} and E_{BC} are the energy gaps of the end-member crystals of AC and BC, respectively, and b is a bowing parameter. According to Hill and Richardson,[43] the bowing parameter for a mixed crystal of $A_xB_{1-x}C$ is composition dependent when the end-members (AC and BC) have different lattice constants and depends on the properties of the intersubstitutional atoms rather than on the structure of the lattice. In the present work, the bowing parameters calculated from eq 1 are 0.43, 0.44, and 0.47 eV for the $Zn_xCd_{1-x}Se$ nanowires of $x = 0.2$, 0.5, and 0.7, respectively. A least-squares fit of the energy gaps, shown in Figure 4b, to the quadratic equation in eq 1 gives

$$E_g(x) = 1.74 + 0.49x + 0.45x^2 \qquad (2)$$

which yields the bowing parameter of $b = 0.45$ eV. The extent of bowing is a measure of the degree of fluctuations in the crystal field or the nonlinear effect that arises due to the anisotropic nature of binding.[41−44] The bowing parameter of $b \sim 0.45$ eV for the $Zn_xCd_{1-x}Se$ alloy nanowires in the present work is quite small as compared with those of other mixed crystals,[41,43] also indicating that ZnSe and CdSe have a good miscibility.

According to a pseudopotential model,[41,43] the value of $b(x)\cdot a(x)^4$ ($a(x)$ is the lattice constant of a ternary $A_xB_{1-x}C$ alloy) should be constant for the alloys with end-members of isostructures. In this work, $b(x)\cdot a(x)^4$ has been calculated 132, 123, and 122 eV Å^4 for the $Zn_xCd_{1-x}Se$ nanowires of $x = 0.2$, 0.5, and 0.7, respectively. On the basis of the pseudopotential model for a II−VI alloy consisting of the end-members of similar structures, Hill and Richardson[44] showed that a plot of $\Delta E\cdot a(x)^4/(1 - x)$ against x should render a straight line passing through the origin, where $\Delta E = E_{LIN} - E_g(x)$ and $E_{LIN} = E_{BC} + (E_{AC} - E_{BC})x$. In the present study, a plot of $\Delta E\cdot a(x)^4/(1 - x)$ vs x indeed shows a line passing through the origin (not shown), thus indicating that the variation of band gaps in the $Zn_xCd_{1-x}Se$ alloy nanowires can be nicely accounted for by the pseudopotential model.

Confocal Raman Spectroscopy. For the phonons in a mixed crystal of ternary alloys, a modified random element isodisplacement (MREI) model developed by Chang and Mitra[30]

TABLE 2: Crystalline Structures, Lattice Spacings, Growth Directions, and Lattice Constants in the $Zn_xCd_{1-x}Se$ Nanowires

composition (x)	crystalline structures	lattice spacing (nm) from HRTEM[a]	growth direction	lattice constants (Å) from SAED	
				a	c
0	wurtzite	0.692 (001)	0 1 −1 0	4.255	6.953
0.2	wurtzite	0.682 (001)	0 1 −1 0	4.180	6.845
0.5	wurtzite	0.670 (001)	0 1 −1 0	4.076	6.697
0.7	zinc blende	0.330 (111)	1 −1 1	5.715	-
1	zinc blende	0.324 (111)	1 −1 1	5.613	-

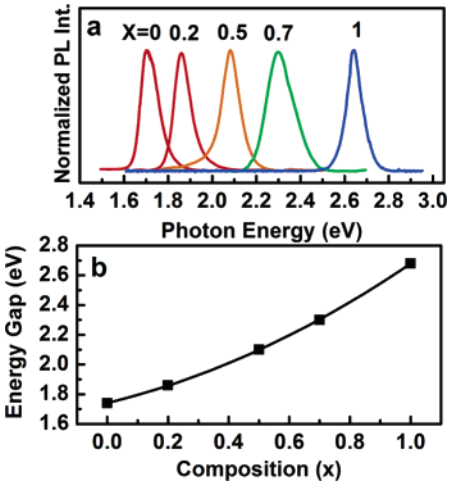

Figure 4. (a) Normalized micro-PL spectra of the $Zn_xCd_{1-x}Se$ nanowires with $x = 0$, 0.2, 0.5, 0.7, and 1. (b) Variation of the energy gaps of $Zn_xCd_{1-x}Se$ nanowires as a function of composition. Solid line represents a least-squares-fitting curve.

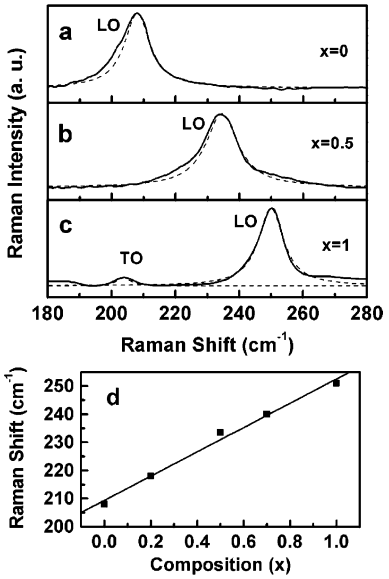

Figure 5. Raman-scattering spectra of (a) CdSe (b) $Zn_{0.5}Cd_{0.5}Se$, and (c) ZnSe nanowires. The dashed Lorentzians, fitted to the observed line shapes, indicate an asymmetric broadening with a low-energy tail developing at higher Cd compositions. fwhm's of the observed line shapes (solid lines)/fitted Lorentzians (dashed lines) are 11.8/9.75 cm^{-1} ($x = 0$), 14.2/12.25 cm^{-1} ($x = 0.5$), and 9.5/9.5 cm^{-1} ($x = 1$). (d) Variation of the Raman shifts as a function of composition in the $Zn_xCd_{1-x}Se$ nanowires.

suggests that the criterion for the existence of the one-mode pattern is that there must not be a substituting element whose mass (m) is smaller than the reduced mass (μ) of the compound formed by the other two elements. In the ternary alloy of $Zn_xCd_{1-x}Se$, since $m_{Cd}(112) > \mu_{ZnSe}(36)$ and $m_{Zn}(65) > \mu_{CdSe}(46)$, one-mode behavior should be exhibited for the phonons in the $Zn_xCd_{1-x}Se$ mixed crystal according to the MREI model.

In parts a−c of Figure 5, Raman-scattering spectra of the $Zn_xCd_{1-x}Se$ nanowires with $x = 0$, 0.5, and 1 are depicted. The Raman shifts at 208 cm^{-1} (Figure 5a) and 251 cm^{-1} (Figure 5c) are attributed to the LO phonon modes of CdSe and ZnSe, respectively.[32,45−48] In previous studies, phonon frequency of the LO mode was observed at 209 cm^{-1} for single-crystalline CdSe quantum dots[49] and is slightly red-shifted to 205 cm^{-1} for CdSe thin film.[45] In single-crystalline ZnSe nanowires, the LO mode has been reported to appear at 250−251 cm^{-1}.[47,48] These phonon frequencies of LO modes agree very well with the present observations. The Raman shift at 204 cm^{-1} in Figure 5c is due to the TO mode in the ZnSe nanowires. This weak TO mode only shows up in the spectra of $Zn_xCd_{1-x}Se$ nanowires with low Cd composition where the TO signal of ZnSe is not embedded in the LO band of CdSe.

In parts a−c of Figure 5, phonon frequency for the LO mode in the $Zn_xCd_{1-x}Se$ nanowires increases as the Cd composition decreases (208 cm^{-1}, $x = 0$; 234 cm^{-1}, $x = 0.5$; 250 cm^{-1}, $x = 1$). Spectral line width of the LO band (solid lines in parts a−c of Figure 5; fwhm = 11.8 cm^{-1}, $x = 0$; 14.2 cm^{-1}, $x = 0.5$; 9.5 cm^{-1}, $x = 1$) increases to a maximum at $x = 0.5$ following the route of a one-mode behavior pattern.[30] The observed LO line shapes become asymmetrically broadened with a low-energy tail developing at higher Cd concentrations, as compared with the fitted Lorentzians (dashed lines in parts a−c of Figure 5; fwhm = 9.75 cm^{-1}, $x = 0$; 12.25 cm^{-1}, $x = 0.5$; 9.5 cm^{-1}, $x = 1$). The asymmetric broadening of the LO phonon band in alloy compounds has also been observed in ZnS_xSe_{1-x}, $In_xGa_{1-x}As$, and $GaInP_2$ crystals reported earlier[50−52] and was conventionally treated with a "spatial correlation" model.[53] In an ideal crystal, the spatial correlation function of the phonon is infinite, which leads to the plane-wave phonon eigenstates and the $q = 0$ selection rule of Raman scattering. For an alloy compound, the asymmetric broadening is caused by alloy potential fluctuation, which removes the translational invariance of the lattice, resulting in a breakdown of the $q = 0$ Raman selection rule and thereby allowing transitions below the LO phonon energy.

In this work, the Raman signals for the LO modes in the $Zn_xCd_{1-x}Se$ alloy nanowires of $x = 0.2$ and 0.7 have also been observed at 218 and 240 cm^{-1}, respectively (not shown). Figure 5d shows the linear variation of the Raman shifts for the LO mode as a function of x in the $Zn_xCd_{1-x}Se$ nanowires and once more exhibits clearly the one-mode behavior pattern.[30] It is noteworthy that the one-mode behavior of LO phonon in the $Zn_xCd_{1-x}Se$ nanowires of the present study is consistent with the LO phonon observed in the $Zn_xCd_{1-x}Se$ ($0 < x < 0.35$) film by Meredith et al.,[54] which also follows quite well the prediction of the MREI model.

4. Conclusions

$Zn_xCd_{1-x}Se$ alloy nanowires have been fabricated in CVD assisted with laser ablation. Crystalline structures and lattice constants of the $Zn_xCd_{1-x}Se$ nanowires in the variation of composition (x) were determined from XRD measurements.

HRTEM and SAED results show that the as-synthesized alloy nanowires are highly single crystalline. These $Zn_xCd_{1-x}Se$ nanowires exhibit strong visible PL from 712 to 463 nm as a nonlinear function of the composition (x) and can serve as important integrated full-color display elements in nanotechnological applications. Energy gaps of the alloy nanowires follow a pseudopotential model with a bowing parameter of ~0.45 eV. Raman-scattering measurements for the LO phonon in the $Zn_xCd_{1-x}Se$ nanowires show that the phonon frequency shifts linearly with the composition and the bandwidth reaches a maximum at $x = 0.5$, demonstrating a one-mode behavior pattern. The successful fabrication of $Zn_xCd_{1-x}Se$ nanowires promises their applications in optical and sensory nanotechnology in the future.

Acknowledgment. Electron microscopic measurements in this study at the Instrumentation Centers of National Taiwan University and National Tsing-Hua University, both sponsored by National Science Council of ROC, are acknowledged. This work is supported by National Science Council of ROC (Grant Nos. 92-2113-M-002-039 and 93-2113-M-002-027).

References and Notes

(1) Wang, Y.; Herron, N. *Chem. Phys. Lett*. **1992**, *200*, 71−75.
(2) Kotov, N. A.; Dekany, I.; Fendler, J. H. *J. Phys. Chem*. **1995**, *99*, 13065−13069.
(3) Mattoussi, H.; Radzilowski, L. H.; Dabbousi, B. O.; Thomas, E. L.; Bawendi, M. G.; Rubner, M. F. *J. Appl. Phys*. **1998**, *83*, 7965−7974.
(4) Colvin, V. L.; Schlamp, M. C.; Alivisatos, A. P. *Nature* **1994**, *370*, 354−357.
(5) Zapien, J. A.; Jiang, Y.; Meng, X. M.; Chen, W.; Au, F. C. K.; Lifshitz, Y.; Lee, S. T. *Appl. Phys. Lett.* **2004**, *84*, 1189−1191.
(6) Brus, L. E. *J. Chem. Phys.* **1984**, *80*, 4403−4409.
(7) Ivanov, S. V. *Phys. Status Solidi A* **2002**, *192*, 157−165.
(8) Che, S. B.; Nomura, I.; Kikuchi. A.; Kishnio, K. *Appl. Phys. Lett*. **2002**, *81*, 972−974.
(9) Tamargo, M. C.; Lin, W.; Guo, S. P.; Guo, Y.; Luo, Y.; Chen, Y. C. *J. Cryst. Growth* **2000**, *214/215*, 1058−1063.
(10) Faschinger, W.; Nürnberger, J. *Appl. Phys. Lett.* **2000**, *77*, 187−189.
(11) Xiang, B.; Zhang, H. Z.; Li, G. H.; Yang, F. H.; Su, F. H.; Wang, R. M.; Xu, J.; Lu, G. W.; Sun, X. C.; Zhao, Q.; Yu, D. P. *Appl. Phys. Lett*. **2003**, *82*, 3330−3332.
(12) Chan, Y. F.; Duan, X. F.; Chan, S. K.; Sou, I. K.; Zhang, X. X.; Wang, N. *Appl. Phys. Lett*. **2003**, *83*, 2665−2667.
(13) Zhang, X. T.; Liu, Z. Leung, Y. P.; Li, Q.; Hark, S. K. *Appl. Phys. Lett*. **2003**, *83*, 5533−5535.
(14) Jiang, Y.; Meng, X.-M.; Yiu, W.-C.; Liu, J.; Ding, J.-X.; Lee, C.-S.; Lee, S.-T. *J. Phys. Chem. B* **2004**, *108*, 2784−2787.
(15) Zhang, X. T.; Ip, K. M.; Liu, Z.; Leung, Y. P.; Li, Q.; Hark, S. K. *Appl. Phys. Lett.* **2004**, *84*, 2641−2643.
(16) Colli, A.; Hofmann, S.; Ferrari, A. C.; Ducati, C.; Martelli, F.; Rubini, S.; Cabrini, S.; Franciosi, A.; Robertson, J. *Appl. Phys. Lett*. **2005**, *86*, 153103.
(17) Xu, D.; Shi, X.; Guo, G.; Gui, L.; Tang, Y. *J. Phys. Chem. B* **2000**, *104*, 5061−5063.
(18) Peng, X.-S.; Zhang, J.; Wang, X.-F.; Wang, Y.-W.; Zhao, L.-X.; Meng, G.-W.; Zhang, L.-D. *Chem. Phys. Lett.* **2001**, *343*, 470−474.
(19) Venugopal, R.; Lin, P.-I.; Liu, C.-C.; Chen, Y.-T. *J. Am. Chem. Soc.* **2005**, *127*, 11262−11268.
(20) Colli, A.; Hofmann, S.; Ferrari, A. C.; Martelli, F.; Rubini, S.; Ducati, C.; Franciosi, A.; Robertson, J. *Nanotechnology* **2005**, *16*, S139−S142.
(21) Shan, C. X.; Liu, Z.; Ng, C. M.; Hark, S. K. *Appl. Phys. Lett*. **2005**, *87*, 033108.
(22) Zhang, X. T.; Liu, Z.; Li, Q.; Hark, S. K. *J. Phys. Chem. B* **2005**, *109*, 17913−17916.
(23) Liu, Y.; Zapien, J. A.; Shan, Y. Y.; Geng, C.-Y.; Lee, C. S.; Lee, S.-T. *Adv. Mater.* **2005**, *17*, 1372−1377.
(24) Huang, Y.; Duan, X.-F.; Lieber, C. M. *Small* **2005**, *1*, 142−147.
(25) Mcalpine, M. C.; Friedman, R. S.; Lieber, C. M. *Proc. IEEE* **2005**, *93*, 1357−1363.
(26) Sirbuly, D. J.; Law, M.; Yan, H.-Q.; Yang, P.-D. *J. Phys. Chem. B* **2005**, *109*, 15190−15213.
(27) Law, M.; Greene, L. E.; Johnson, J. C.; Saykally, R.; Yang, P.-D. *Nat. Mater.* **2005**, *4*, 455−459.
(28) Van-Vechten, J. A.; Bergstresser, T. K. *Phys. Rev. B.* **1970**, *1*, 3351−3358.
(29) Richardson, D. *J. Phys. C: Solid State Phys*. **1971**, *4*, L289−292.
(30) Chang, I. F.; Mitra, S. S. *Phys. Rev*. **1968**, *172*, 924−933.
(31) Yang, Y. H.; Wu, S. J.; Chiu, H. S.; Lin, P. I.; Chen, Y. T. *J. Phys. Chem. B* **2004**, *108*, 846−852.
(32) Glinka, Y. D.; Lin, S. H.; Chen, Y. T. *Phys. Rev. B* **2002**, *66*, 035404 and references therein.
(33) Miao, J. Y.; Hwang, D. W.; Narasimhulu, K. V.; Lin, P. I.; Chen, Y. T.; Lin, S. H.; Hwang, L. P. *Carbon* **2004**, *42*, 813−822.
(34) Liu, Y. C.; Lin, P. I.; Chen, Y. T.; Ger, M. D.; Lan, K. L.; Lin, C. L. *J. Phys. Chem. B* **2004**, *108*, 14897−14900.
(35) Power-dependence measurements for the Raman-scattering signals of CdSe nanobelts and sheets can be found in the Supporting Information of ref 19, in which neither peak shift nor band broadening could be observed at the laser intensity of ≤70 kW/cm^2.
(36) Hotje, U.; Rose, C.; Binnewises, M. *Solid State Sci*. **2003**, *5*, 1259−1262.
(37) Zhang, Z. Y.; Yong, X. Y.; Xiao, M. *Appl. Phys. Lett*. **2002**, *81*, 2076−2078.
(38) Cherin, P.; Lind, E. L.; Dais, E. A. *J. Electrochem. Soc.* **1970**, *117*, 233−236.
(39) Shimaoka, G.; Suzuki, Y. *Appl. Surf. Sci.* **1997**, *113/114*, 528−533.
(40) Wagner, R. S.; Ellis, W. C. *Appl. Phys. Lett.* **1964**, *4*, 89−90.
(41) Hill, R. *J. Phys. C: Solid State Phys*. **1974**, *7*, 521−526.
(42) Richardson, D.; Hill, R. *J. Phys. C: Solid State Phys*. **197**2, *5*, 821−827.
(43) Richardson, D.; Hill, R. *J. Phys. C: Solid State Phys*. **1973**, *6*, L115−L119.
(44) Hill, R.; Richardson, D. *Thin Solid Films* **1973**, *18*, 25−28.
(45) Rai, B. K.; Bist, H. D.; Katiyar, R. S.; Nair, M. T. S.; Nair, P. K.; Mannivannan, A. *J. Appl. Phys.* **1997**, *82*, 1310−1319.
(46) Hwang, Y. N.; Park, S. H.; Kim, D. *Phys. Rev. B* **1999**, *59*, 7285−7288.
(47) Xiang, B.; Zhnag, H. Z.; Li, G. H.; Yang, F. H.; Su, F. H.; Wang, R. M.; Xu, J.; Lu, G. W.; Sun, X. C.; Zhao, Q.; Yu, D. P. *Appl. Phys. Lett*. **2003**, *82*, 3330−3332.
(48) Jiang, J.; Meng, X. M, Yiu, W. C.; Ding, J. X.; Kee, C. S.; Lee, S. T. *J. Phys. Chem. B* **2004**, *108*, 2784−2787.
(49) Hwang, Y.; Shin, S.; Park, H.; Park, S.; Kim, U.; Jeong, H.; Shin, E.; Kim, D. *Phys. Rev. B* **1996**, *54*, 15120−15124.
(50) Pal, A. J.; Mandal, J. *J. Alloy Compd.* **1994**, *216*, 265−267.
(51) Shen, J. L.; Chang, I. M.; Shu, Y. M.; Chen, Y. F.; Chang, S. Z.; Lee, S. C. *Phys. Rev. B* **1994**, *50*, 1678−1683.
(52) Sinha, K.; Mascarenhas, A.; Horner, G. S.; Bertness, K. A.; Kurtz, S. R.; Olson, J. M. *Phys. Rev. B* **1994**, *50*, 7509−7513.
(53) Parayanthal, P.; Pollak, F. H. *Phys. Rev. Lett.* **1984**, *52*, 1822−1825.
(54) Meredith, W.; Horsburgh, G.; Brownlie, G. D.; Prior, K. A.; Cavenett, B. C.; Rothwell, W.; Dann, A. *J. Cryst. Growth*. **1996**, *159*, 103−107.